Multi-aspect POL-InSAR 3D Urban Scene Reconstruction at L-Band

S. Sauer[1], L. Ferro-Famil[1], A. Reigber[2], E. Pottier[1]

[1] University of Rennes 1, IETR Laboratory, SAPHIR Team, Bat. 11D, 263 Avenue General Leclerc, CS 74205, 35042 Rennes Cedex, France, Tel./Fax: ++33-223-235019 / 236963, Email: stefan.sauer@univ-rennes1.fr
[2] German Aerospace Center, Microwaves and Radar Institute, Oberpfaffenhofen-Wessling, Germany, Tel./Fax: +49 8153 28-2360 / 1449

Abstract

This paper generalizes a multibaseline interferometric SAR signal model to the polarimetric scenario. Based on this formulation, three spectral analysis techniques are adapted to process multibaseline POL-InSAR observations. These new methods enhance the height estimation of scatterers by calculating optimal polarization combinations and allow the determination of their polarimetric reflectivities and physical characteristics. Building layover is analyzed by producing three-dimensional images from polarimetric dual-baseline InSAR measurements. The dataset has been acquired by DLR's E-SAR system over Dresden city.

1 Introduction

Recently, spectral analysis techniques have been utilized for three-dimensional imaging from single polarization dual-baseline observations [1] and polarimetric tomographic measurements [2, 3]. A 3D radar imaging technique of vegetation using single and dual-baseline POL-InSAR data called polarization coherence tomography has been developed in [4]. This paper presents a new way of analyzing polarimetric multibaseline (MB) InSAR signals by adapting three array signal processing techniques to this configuration [5, 6]. In section 2, the conventional single polarization signal model, the classical beamforming, Capon, and MUSIC algorithms for MB InSAR height and reflectivity estimation are outlined. Section 3 describes the generalization to the fully polarimetric MB InSAR set-up: The signal model is adapted to deal with four polarization channels and subsequently the polarimetric beamforming, Capon, and MUSIC methods are formulated in a rigorous mathematical way and their features are described. Finally, experimental results are shown in section 4: The methods are applied to produce three-dimensional images of building layover by means of polarimetric dual-baseline InSAR data. The dataset has been acquired by DLR's E-SAR system over Dresden city.

2 Classical Spectral Analysis Algorithms

This section describes a single polarization multibaseline InSAR signal model and three conventional spectral analysis techniques: The beamforming, Capon, and MUSIC algorithms.

2.1 Multibaseline InSAR Signal Model

The single polarization multibaseline InSAR received signal with p sensors can be modeled as

$$\begin{aligned}\mathbf{y}(n) &= \mathbf{t} + \mathbf{c}(n) + \mathbf{v}(n) \\ &= \sum_{i=1}^{N_{s_t}} \sqrt{\tau_{t_i}} \exp(j\psi_i)\mathbf{a}(z_{t_i}) \\ &+ \sum_{j=1}^{N_{s_c}} \sqrt{\tau_{c_j}} \mathbf{x}_j(n) \odot \mathbf{a}(z_{c_j}) + \mathbf{v}(n) \qquad (1)\end{aligned}$$

with $n = 1, \ldots, N$, the number of looks N, and the Schur-Hadamard product $\odot$ (elementwise multiplication). The MB InSAR received data vector $\mathbf{y}(n) \in \mathbb{C}^p$ is assumed to be a Gaussian random process with nonzero mean and covariance matrix $\mathbf{R} \in \mathbb{C}^{p\times p}$, i.e. $\mathbf{y}(n) \sim \mathcal{N}_{\mathbb{C}}(\boldsymbol{\mu}, \mathbf{R})$. The first term, $\mathbf{t}$, is highly coherent and can be associated to a deterministic or almost deterministic target [7]. The second contribution, $\mathbf{c}(n)$, represents the response of distributed environments including the SAR speckle effect as multiplicative noise [8]. The additive white Gaussian noise $\mathbf{v}(n) \in \mathbb{C}^p$ has zero mean and power σ_v^2, i.e. $\mathbf{v}(n) \sim \mathcal{N}_{\mathbb{C}}(\mathbf{0}, \sigma_v^2\mathbf{I})$. The number of backscattering sources N_{s_t} and N_{s_c} of the coherent and incoherent component, respectively, are assumed to be known. The total number of scatterers is $N_s = N_{s_t} + N_{s_c}$. The reflectivity τ and the height z of the scatterers as well as the complex argument ψ are considered to be deterministic unknown quantities. The steering vector $\mathbf{a}(z) \in \mathbb{C}^p$ for a general acquisition geometry is represented as

$$\mathbf{a}(z) = [1, \exp(j\kappa_{z_2} z), \ldots, \exp(j\kappa_{z_p} z)]^T \qquad (2)$$

with the vertical wavenumber $\kappa_{z_i} = \frac{4\pi}{\lambda}\frac{B_\perp^{(i)}}{r^{(i)}\sin\theta^{(i)}}$. The multiplicative noise $\mathbf{x}_i(n) \in \mathbb{C}^p$ is a Gaussian random vector with zero mean and covariance matrix $\mathbf{C}_i =$

$E\{\mathbf{x}_i(n)\mathbf{x}_i^H(n)\}$ where H denotes transpose, complex conjugate. This model does not take multipath effects into account. The sample covariance matrix $\hat{\mathbf{R}} \in \mathbb{C}^{p\times p}$ is computed by

$$\hat{\mathbf{R}} = \frac{1}{N}\sum_{n=1}^{N}\mathbf{y}(n)\mathbf{y}^H(n). \quad (3)$$

2.2 Conventional Beamforming

The spectrum of the beamforming method is obtained as

$$\hat{P}_{BF}(z) = \frac{\mathbf{a}^H(z)\hat{\mathbf{R}}\mathbf{a}(z)}{p^2}. \quad (4)$$

The frequency estimates $\hat{\boldsymbol{z}} = [\hat{z}_1, \ldots, \hat{z}_{N_s}]^T$ correspond to the locations of the N_s maxima of the spectrum. The reflectivity estimate at frequency $\hat{z}_i$ is determined by $\hat{\tau}_i = \hat{P}_{BF}(\hat{z}_i)$.

2.3 Capon Method

The Capon spectrum is given by [9]

$$\hat{P}_C(z) = \frac{1}{\mathbf{a}^H(z)\hat{\mathbf{R}}^{-1}\mathbf{a}(z)} \quad (5)$$

where $\hat{\mathbf{R}}^{-1}$ is the inverse matrix. The frequency estimates $\hat{\boldsymbol{z}} = [\hat{z}_1, \ldots, \hat{z}_{N_s}]^T$ are associated with the frequencies of the N_s highest peaks of the spectrum $\hat{P}_C$. The reflectivity at frequency $\hat{z}_i$ is estimated by $\hat{\tau}_i = \hat{P}_C(\hat{z}_i)$.

2.4 Classical MUSIC Algorithm

Let N_s denote the supposed total number of scatterers. Then the number of eigenvalues of the noise subspace equals $q = p - N_s$, and the matrix $\mathbf{E}_q \in \mathbb{C}^{p\times q}$ of the corresponding eigenvectors spans this subspace. The pseudospectrum of the single polarization MUSIC method [10] can be calculated by

$$\hat{P}_{MU}(z) = \frac{1}{\mathbf{a}^H(z)\mathbf{E}_q\mathbf{E}_q^H\mathbf{a}(z)}. \quad (6)$$

The spectrum peak locations indicate the height of the scatterers. The subspace spanned by the noise eigenvectors must be at least of dimension one ($p \geq N_s + 1$).

3 Polarimetric Multibaseline InSAR Spectral Analysis Algorithms

In this section, the spectral analysis techniques are extended to the fully polarimetric MB InSAR configuration. In this situation, the antennas not only receive the signals in diverse polarizations [11, 10], but emit the electromagnetic waves and receive the echo in polarimetric mode. The following adaptation to the fully polarimetric case not merely increases the number of observables, but especially finds the optimal polarization combination for height estimation. Furthermore, these algorithms allow examining the scatterer physical properties by analysis of their polarimetric behavior.

3.1 Polarimetric MB InSAR Signal Model

The signal model for multibaseline InSAR data described in section 2 has to be generalized to take polarization diversity into account. The polarimetric multibaseline interferometric SAR received signal for p sensors is modeled as:

$$\begin{aligned}\mathbf{y}(n) &= \sum_{i=1}^{N_{s_t}}\sqrt{\tau_{t_i}}\exp(j\psi_i)\mathbf{b}(z_{t_i},\mathbf{k}_{t_i}) \\ &+ \sum_{j=1}^{N_{s_c}}\sqrt{\tau_{c_j}}\mathbf{x}_j(n)\odot\mathbf{b}(z_{c_j},\mathbf{k}_{c_j}) + \mathbf{v}(n). \quad (7)\end{aligned}$$

The observation vector $\mathbf{y}(n) \in \mathbb{C}^{\tilde{p}}$, $\tilde{p} = 4p$, is a Gaussian random process with nonzero mean and covariance matrix $\mathbf{R} \in \mathbb{C}^{\tilde{p}\times\tilde{p}}$, i.e. $\mathbf{y}(n) \sim \mathcal{N}_{\mathbb{C}}(\boldsymbol{\mu}, \mathbf{R})$. The main modification with respect to the single polarization model is the structure of the MB polarimetric interferometric (MBPI) steering vector $\mathbf{b}(z,\mathbf{k}) \in \mathbb{C}^{\tilde{p}}$. It is a linear combination of several steering vectors $\mathbf{a}_{\gamma_i}(z) \in \mathbb{C}^{\tilde{p}}$, each of them associated to one particular polarization:

$$\mathbf{b}(z,\mathbf{k}) = k_1\mathbf{a}_{\gamma_1}(z) + k_2\mathbf{a}_{\gamma_2}(z) + k_3\mathbf{a}_{\gamma_3}(z) + k_4\mathbf{a}_{\gamma_4}(z). \quad (8)$$

The weighting coefficients $k_i \in \mathbb{C}$ form a vector

$$\mathbf{k} = [k_1, k_2, k_3, k_4]^T \in \mathbb{C}^4 \quad (9)$$

that may be interpreted as a scattering mechanism. This can be written in matrix notation as

$$\mathbf{b}(z,\mathbf{k}) = \mathbf{B}(z)\mathbf{k} \quad (10)$$

with the matrix of MBPI steering vectors $\mathbf{B}(z) \in \mathbb{C}^{\tilde{p}\times 4}$

$$\mathbf{B}(z) = \left[\mathbf{a}_{\gamma_1}(z), \mathbf{a}_{\gamma_2}(z), \mathbf{a}_{\gamma_3}(z), \mathbf{a}_{\gamma_4}(z)\right]. \quad (11)$$

3.2 Polarimetric Beamforming

The spectrum of the polarimetric beamforming method is given by

$$\hat{P}_{BF}^{P}(z) = \frac{\lambda_{\max}(\mathbf{B}^H(z)\hat{\mathbf{R}}\mathbf{B}(z))}{p^2} \quad (12)$$

where $\lambda_{\max}(\cdot)$ is the maximum eigenvalue operator. This means that for each frequency z the maximal eigenvalue and its corresponding eigenvector of the linear system

$$\mathbf{B}^H(z)\hat{\mathbf{R}}\mathbf{B}(z)\mathbf{k}_{\max} = \lambda_{\max}\mathbf{k}_{\max} \quad (13)$$

has to be computed. The eigenvector $\mathbf{k}_{\max}$ can be interpreted as a polarimetric scattering mechanism allowing a

polarimetric analysis to retrieve the physical properties of the reflector. The frequency estimates $\hat{\boldsymbol{z}} = [\hat{z}_1, \ldots, \hat{z}_{N_s}]^T$ are related to the positions of the N_s largest peaks of the spectrum. The polarimetric reflectivity at frequency $\hat{z}_i$ is estimated by $\hat{\tau}_i = \hat{P}^P_{BF}(\hat{z}_i)$.

3.3 Polarimetric Capon Method

The spectrum of the polarimetric Capon algorithm is obtained as

$$\hat{P}^P_C(z) = \frac{1}{\lambda_{\min}(\mathbf{B}^H(z)\hat{\mathbf{R}}^{-1}\mathbf{B}(z))} \tag{14}$$

where $\lambda_{\min}(\cdot)$ is the minimum eigenvalue operator. For each frequency z the minimal eigenvalue and associated eigenvector of the linear system

$$\mathbf{B}^H(z)\hat{\mathbf{R}}^{-1}\mathbf{B}(z)\mathbf{k}_{\min} = \lambda_{\min}\mathbf{k}_{\min} \tag{15}$$

has to be calculated. The polarimetric scattering type $\mathbf{k}_{\min}$ permits to extract the physical behavior of the scatterer. The frequency estimates $\hat{\boldsymbol{z}} = [\hat{z}_1, \ldots, \hat{z}_{N_s}]^T$ are given by the locations of the N_s maxima of the spectrum $\hat{P}^P_C$. The polarimetric reflectivity at frequency $\hat{z}_i$ is extracted by $\hat{\tau}_i = \hat{P}^P_C(\hat{z}_i)$.

3.4 Polarimetric MUSIC Algorithm

If N_s is the assumed number of scatterers, the matrix of the noise eigenvectors is $\mathbf{E}_q \in \mathbb{C}^{\tilde{p}\times q}$ with $q = \tilde{p} - N_s$. The spectrum of MUSIC for the fully polarimetric SAR configuration is

$$\hat{P}^P_{MU}(z) = \frac{1}{\lambda_{\min}(\mathbf{B}^H(z)\mathbf{E}_q\mathbf{E}_q^H\mathbf{B}(z))} \tag{16}$$

with $\lambda_{\min}$ the smallest eigenvalue of the 4×4 Hermitian linear system

$$\mathbf{B}^H\mathbf{E}_q\mathbf{E}_q^H\mathbf{B}\mathbf{k}_{\min} = \lambda_{\min}\mathbf{k}_{\min}. \tag{17}$$

The eigenvector $\mathbf{k}_{\min}$ describes the physical features of the scatterer and permits a polarimetric analysis. The linear system (17) must be of full rank, otherwise $\lambda_{\min} = 0$. This leads to an infinite spectrum (16) and the height cannot be determined. A necessary criterion for the linear system having full rank is $\tilde{p} \geq N_s + 4$.

4 Experimental Results

To demonstrate the performance of the above introduced algorithms, building layover is analyzed by producing three-dimensional images from dual-baseline POL-InSAR measurements. The baselines of approximately 10 m and 40 m lead to a height of ambiguity of $H^{sb}_{amb} \approx 67.5$ m and $H^{lb}_{amb} \approx 15$ m, respectively. Tomographic slices are calculated by the beamforming and Capon methods using observations in vv channel and with polarization diversity. The single polarization and fully polarimetric MUSIC algorithms produce pseudo-tomograms. The three-dimensional images have been computed in the range $[-10\text{ m}, 25\text{ m}]$ in the vertical direction. The tomographic slice shown in **Figure 1** is calculated by the single polarization (SP) beamforming algorithm. On the right hand side, the backscattering from the wall-ground interaction at the topographic height of approximately 0 m is clearly visible. The sidelobes are rather strong. In the middle of the 3D image, the SP Beamformer shows reflectors between 10 and 15 m and high sidelobes below 0 m. Compared to the very strong backscattering from the wall-ground interaction, the reflectivity is weak at the left hand side.

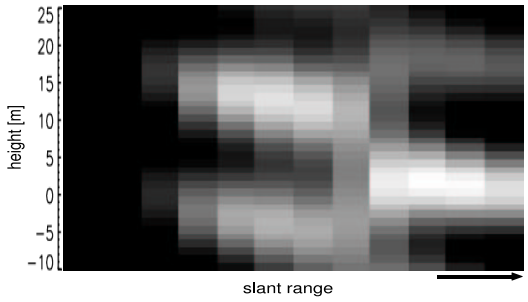

Figure 1: Three-dimensional imaging of building layover. The x-axis corresponds to the slant range with far range on the right hand side. The y-axis is related to the estimated height going from -10 m to 25 m. Single polarization beamforming tomographic slice.

The three-dimensional imaging result of the fully polarimetric (FP) Capon technique is illustrated in **Figure 2**. On the right side, the Capon algorithm detects a signal at around 0 m. The sidelobes are conspicuously reduced. Going to the left, the FP Capon separates two contributions, the first slightly above 0 m, and the second at approximately 15 m related to the building height. Again, on the left side, the backscattering is very weak. In comparison with the beamforming method, the Capon algorithm leads to finer resolution and better leakage reduction. To a limited extent, the fully polarimetric Capon technique possesses sufficiently narrow peaks to identify two contributions at different height locations.

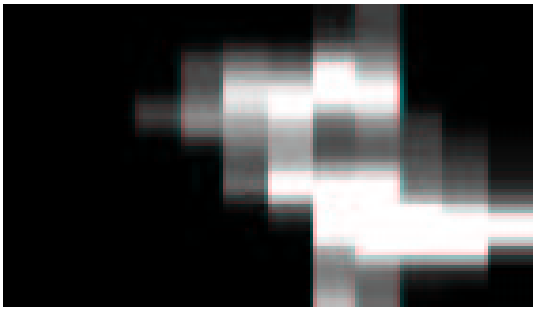

Figure 2: Fully polarimetric Capon tomographic slice.

The pseudo-tomograms of the single polarization and fully polarimetric MUSIC methods with fixed model order one are shown in **Figure 3** and **Figure 4**, respectively. Both algorithms are appropriate to recognize one reflector at around 0 m at the right hand side. The sidelobes are significantly diminished. While the height of the main scatterer rises from around 11 m to 18 m in the SP MUSIC image, the elevation of the main reflector of the FP MUSIC method is very stable at approximately 17 m. The behavior of the second peak at around -2 m (SP) and 0 m (FP) is similar. Compared to the beamforming and Capon techniques, the spectral peaks of MUSIC with model order one are very narrow and the sidelobes are visibly decreased.

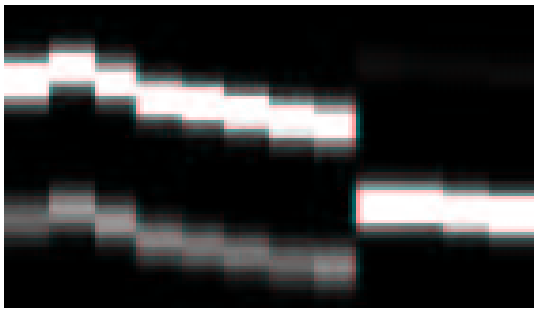

Figure 3: Single polarization MUSIC pseudo-tomographic slice, model order fixed to one.

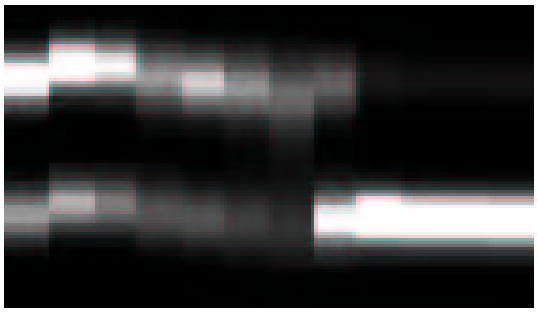

Figure 4: Fully polarimetric MUSIC pseudo-tomographic slice, model order fixed to one.

5 Conclusion

This paper has introduced three spectral analysis techniques to process fully polarimetric multibaseline interferometric SAR observations. They optimize the polarizations for scatterer height estimation and permit the determination of their polarimetric reflectivities and physical behavior. The proposed techniques are applied to generate three-dimensional images of building layover from dual-baseline POL-InSAR measurements. In the future the optimal polarimetric scattering mechanisms will be examined in detail.

References

[1] F. Lombardini, L. Rössing, J. Ender, F. Viviani: *Towards a Complete Processing Chain of Multibaseline Airborne InSAR Data for Layover Scatterers Separation*, Proceedings of URBAN'07, April 2007.

[2] F. Lombardini, A. Reigber: *Adaptive Spectral Estimation for Multibaseline SAR Tomography with Airborne L-band Data*, Proceedings of IGARSS'03, July 2003.

[3] S. Guillaso, M. Jäger, A. Reigber: *Information Extraction from Tomographic SAR Data*, Proceedings of EUSAR'06, May 2006.

[4] S. R. Cloude: *Dual-baseline coherence tomography*, IEEE Geoscience and Remote Sensing Letters, vol. 4, no. 1, pp. 127-131, Jan. 2007.

[5] S. Sauer, L. Ferro-Famil, A. Reigber, E. Pottier: *3D Visualisation and Physical Feature Extraction of Urban Areas using Multibaseline POL-InSAR Data at L-Band*, Proceedings of URBAN'07, April 2007.

[6] S. Sauer, L. Ferro-Famil, A. Reigber, E. Pottier: *Multibaseline POL-InSAR Analysis of Urban Scenes for 3D Modeling and Physical Feature Retrieval at L-Band*, Proceedings of IGARSS'07, July 2007.

[7] L. Ferro-Famil, A. Reigber, E. Pottier: *Study and Applications of POLSAR Data Time-Frequency Correlation Properties*, Proceedings of POL-InSAR'07, Jan. 2007.

[8] F. Lombardini, M. Montanari, F. Gini: *Reflectivity Estimation for Multibaseline Interferometric Radar Imaging of Layover Extended Sources*, IEEE Trans. on Signal Processing, vol. 51, pp. 1508-1519, June 2003.

[9] J. Capon: *High-resolution frequency-wavenumber spectrum analysis*, Proceedings of the IEEE, vol. 57(8), pp. 1408-1418, 1969.

[10] R. O. Schmidt: *Multiple Emitter Location and Signal Parameter Estimation*, Proc. RADC Estimation Workshop, Rome Air Development Center, N.Y., Oct. 1979.

[11] E. R. Ferrara, T. M. Parks: *Direction Finding with an Array of Antennas Having Diverse Polarizations*, IEEE Trans. on Antennas and Propagation, vol. 31, pp. 231-236, March 1983.